Image Synthesis by Rank-1 Lattices

S. Dammertz and A. Keller
Institute of Media Informatics, Ulm University, Germany

Abstract

Considering uniform points for sampling, rank-1 lattices provide the simplest generation algorithm. Compared to classical tensor product lattices or random samples, their geometry allows for a higher sampling efficiency. These considerations result in a proof that for periodic Lipschitz continuous functions, rank-1 lattices with maximized minimum distance perform best. This result is then investigated in the context of image synthesis, where we study anti-aliasing by rank-1 lattices and using the geometry of rank-1 lattices for sensor and display layouts.

1 Introduction

Image synthesis can be considered as an integro-approximation problem

$$I(k,l) := \int_{I^s} f(\mathbf{x},k,l)d\mathbf{x} \approx \frac{1}{n}\sum_{i=0}^{n-1} f(\mathbf{x}_i,k,l), \tag{1}$$

where the two-dimensional image function $I(k,l)$ is given by a parametric integral. Since usually analytic solutions are hardly accessible, we are interested in efficient numerical schemes to approximate the image function. Thinking of (k,l) as pixel coordinates on the screen, the above algorithm simultaneously computes a color for each pixel on the screen by averaging samples of the integrand at positions $\mathbf{x}_i$. We consider two important aspects:

Sampling: In computer graphics the accumulation buffer [HA90] along with several extensions and improvements [Kel97, KH01, SIP06] is the most efficient implementation of integro-approximation as it can take advantage of the vast performance of rasterization hardware. In the original article [HA90] sampling points $\mathbf{x}_i$ generated by Lloyd relaxation were found to perform best. This implies that sampling points should have maximized minimum distance.

Display: Modern displays use either rectangular or hexagonal arrangements of pixels. Again, due to a larger minimum distance hexagonal arrangements expose a much better visual quality than rectangular arrangements, nevertheless, image synthesis is currently still dominated by the first.

As we will show in the following, rank-1 lattices selected by maximized minimum distance approximate hexagonal lattices. However, rank-1 lattices are simpler to generate and exist for any number of points in any dimension. We investigate the application of such lattices in two dimensions for anti-aliasing and display and sensor technology.

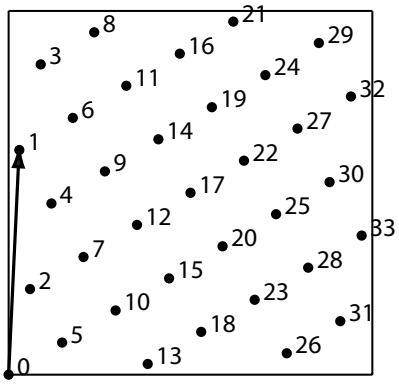

Figure 1: The $n = 34$ points of the Fibonacci lattice $L_{34,21}$ with generator vector $\mathbf{g} = (1, 21)$.

2 Geometry of Rank-1 Lattices

A lattice L is a discrete subset of $\mathbb{R}^s$ which is closed under addition and subtraction. Given an s-dimensional lattice basis $\{\mathbf{b}_1, \ldots, \mathbf{b}_s\}$, the lattice can be generated by all integer linear combinations

$$L(\mathbf{b}_1, \ldots, \mathbf{b}_s) := \left\{ \sum_{j=1}^{s} \lambda_j \mathbf{b}_j : \lambda_1, \ldots, \lambda_s \in \mathbb{Z} \right\}. \tag{2}$$

Of all possible bases the Minkowski-reduced bases, which contain the s shortest linearly independent vectors of L [AEVZ02], are the most useful for our purpose.

Instead of using s basis vectors the points $\mathbf{x}_i$ of a rank-1 lattice [Nie92b, SJ94]

$$L_{n,\mathbf{g}} := \left\{ \mathbf{x}_i := \frac{i}{n}\mathbf{g} \bmod 1 : i = 0, \ldots, n-1 \right\}$$

in the unit cube are easily generated by using only one suitable generator vector $\mathbf{g} \in \mathbb{N}^s$ for a fixed number $n \in \mathbb{N}$ of points. Korobov lattices $L_{n,a}$ are a special class of rank-1 lattices. Their generator vector has the form $\mathbf{g} = (1, a, a^2, \ldots, a^{s-1})$. The Fibonacci lattices are an instance of a two-dimensional Korobov lattice. Based on the Fibonacci sequence $F_k := F_{k-1} + F_{k-2}$ with $F_2 := F_1 := 1$, the number of points is set to $n = F_k, k \geq 2$ and the generator vector is defined as $\mathbf{g} = (1, F_{k-1})$. Figure 1 shows a Fibonacci lattice in the unit square with $n = F_9 = 34$ points and the generator vector $\mathbf{g} = (1, F_8) = (1, 21)$.

The generator vector $\mathbf{g}$ of a rank-1 lattice can be chosen such that the resulting point set is of low discrepancy [SJ94]. Then the elements of this point set are called good lattice points. But only very few explicit constructions for good lattice points exist. Similar to the Fibonacci lattices Niederreiter and Borosh [BN83, Nie86] showed that good two-dimensional lattice points can be explicitly constructed for n being a power of two.

Obviously the quality of rank-1 lattices is significantly influenced by their integer generator vector $\mathbf{g}$. For lattices in Korobov form the search is reduced to only one parameter a.

2.1 Shifted Rank-1 Lattices

Considering shifted rank-1 lattices

$$L^{\mathbf{\Delta}}_{n,\mathbf{g}} := \left\{ \mathbf{x}_i := \frac{i}{n}\mathbf{g} + \mathbf{\Delta} \bmod 1 : \mathbf{\Delta} \in \mathbb{R}^s; i = 0, \ldots, n-1 \right\}$$

there exists a trivial, but nevertheless interesting connection to $(t, m, s)-$nets in basis b [Nie92b].

$(0, 2, 2)$-nets in base b only exhibit three kinds of elementary intervals

$$\begin{aligned} \left[\frac{i}{b}, \frac{i+1}{b}\right) \times \left[\frac{j}{b}, \frac{j+1}{b}\right) \quad &\text{for} \quad 0 \leq i, j < b, \\ \left[\frac{i}{b^2}, \frac{i+1}{b^2}\right) \times \left[0, 1\right) \quad &\text{for} \quad 0 \leq i < b, \text{ and} \\ \left[0, 1\right) \times \left[\frac{i}{b^2}, \frac{i+1}{b^2}\right) \quad &\text{for} \quad 0 \leq i < b, \end{aligned}$$

whereof each must contain exactly one of the $n = b^2$ points of the shifted rank-1 lattice due to $t = 0$. The latter two kinds of intervals guarantee perfect one-dimensional projections. Independent of the shift $\mathbf{\Delta}$, this is obtained by requiring $\gcd(n, g_i) = 1, i \in \{1, \ldots, s\}$. Possible shift coordinates are given by the one-dimensional projections of the lattice points. It is sufficient to search shifts in only one of the elementary intervals, such that the $t = 0$ condition is fulfilled. An illustration for $L^{\mathbf{\Delta}}_{25,7}$ with $\mathbf{\Delta} = (\frac{2}{25}, \frac{2}{25})$ is found in Figure 2 and further parameters are listed in Table 1.

Like $(0, 2, 2)-$nets the resulting lattices share both the properties of jittered grid and Latin hypercube samples but can be computed faster due to a simpler algorithm.

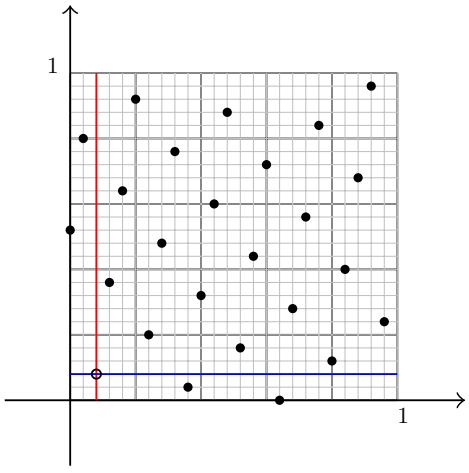

Figure 2: Example of a shifted rank-1 lattice $L^{\mathbf{\Delta}}_{25,7}$ with $\mathbf{\Delta} = (\frac{2}{25}, \frac{2}{25})$ that is a $(0, 2, 2)$-net in basis $b = 5$.

b	$n = b^2$	a	$n \cdot \mathbf{\Delta} \in [0, b)^2]$
2	4	1	$(1, 0)$
3	9	2	$(1, 1)$
5	25	7	$(2, 2)$
7	49	6	$(5, 1)$
11	121	36	$(5, 5)$
13	169	70	$(6, 6)$
17	289	80	$(2, 4)$
19	361	100	$(14, 15)$
23	529	120	$(0, 2)$
29	841	150	$(7, 8)$
31	961	210	$(7, 9)$

Table 1: Parameters for shifted rank-1 lattices in Korobov form that are $(0, 2, 2)$-nets in base b. The rational shift $\mathbf{\Delta}$ is scaled by n for integer precision.

2.2 Maximized Minimum Distance Rank-1 Lattices

In computer graphics sampling patterns with blue noise spectral properties are used in analogy to the principle of maximized minimum distance apparent in nature. For example the photo

receptors in the retina are distributed according to this scheme [Yel83] in order to reduce aliasing.

Similarly we can select rank-1 lattice generator vectors that maximize the minimum distance, which leads to the notion of maximized minimum distance lattices. The task of calculating the minimum distance in a lattice is a well known problem in lattice theory, namely the shortest vector problem [AEVZ02]. Since a lattice is closed under addition and subtraction the difference between two lattice points yields another point in the lattice. Therefore the minimum distance corresponds to the length of the shortest vector in the lattice. This quantity can be computed by searching the closest point to the origin, which means to consider all lattice points except $\mathbf{x}_0 = \mathbf{0}$.

For $s = 2$ the sequence of rank-1 lattices with increasing minimum distance approximates the hexagonal lattice in the limit, which is illustrated in Figure 3 for $n = 144$ points.

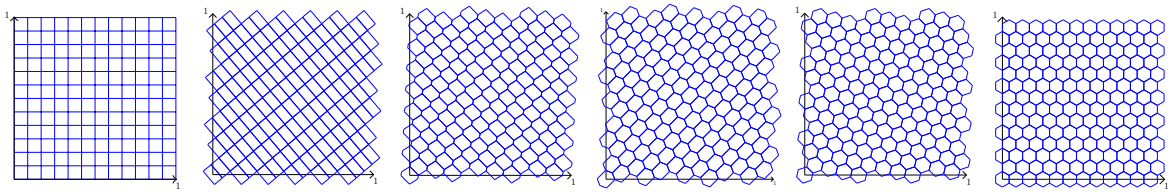

rect. lattice $L_{144,42}$ $L_{144,19}$ $L_{144,89}$ $L_{144,33}$ hex. lattice

Figure 3: In the sequence of Korobov lattices $L_{144,a}$ the minimum distance increases from left to right. For comparison the rectangular lattice is added to the left, whereas the hexagonal lattice is the rightmost of the image sequence.

In [CR97] Cools and Reztsov define a family

$$L_{n,\mathbf{g}} = \left\{ \frac{i}{2F_m M_m} (M_m, F_m) \bmod 1 : 0 \leq i < 2F_m M_m \right\} \tag{3}$$

of rank-1 lattices by using the sequence of convergents

$$\left\{ \frac{F_m}{M_m} \right\}_{m=1}^{\infty} = \frac{2}{1}, \frac{5}{3}, \frac{7}{4}, \frac{19}{11}, \ldots$$

of the continued fraction equal to $\sqrt{3}$. Since these lattices are constructed to exactly integrate trigonometric polynomials of a hexagonal spectrum, they actually represent maximized minimum distance lattices. As the construction only covers lattices for $n = 2F_m M_m$ points, for other n the generator vector was determined by computer search.

2.2.1 Computer Search

Searching for maximized minimum distance rank-1 lattices represents a computationally expensive problem, since there are $(n-1)^s$ possibilities for the generator vector $\mathbf{g} = (g_1, \ldots, g_s)$, where $g_i \in \{1, \ldots, n-1\}$. However, for $s = 2$ an exhaustive search is feasible. In order to avoid rounding errors due to floating point imprecision all computations are done in integer arithmetic allowing for exact results.

One possibility to reduce the search space is to consider only rank-1 lattices in Korobov form, which are uniquely determined by the tuple (n, a) (see Section 2). A very efficient way to search for maximized minimum distance lattices in Korobov form for $s = 2$ is given by the spectral test [Knu81], which measures the quality of linear congruential random number generators by determining the t-dimensional accuracy ν_t. It can be shown that this quantity corresponds to the length of the shortest vector in the dual lattice

$$L^{\perp}_{n,\mathbf{g}} := \{\mathbf{h} \in \mathbb{Z}^s : \mathbf{h} \cdot \mathbf{g} \equiv 0 \pmod{n}\}.$$

Since the length of the shortest vector in $L^{\perp}$ equals the length of the shortest vector in L multiplied by n, the spectral test delivers the minimum mutual distance between two lattice points for one $a \in \{1, \ldots, n-1\}$ on $[0, n)^2$. As the searching algorithm is performed on $[0, n)^2$, the two-dimensional accuracy ν_2 delivers the sought quantity, i.e. the length of the shortest vector in the lattice $L_{n,a}$.

Additionally, the search space can be restricted by demanding that n and g_i are relatively prime, i.e. $\gcd(n, g_i) = 1$. This means that the resulting lattice points will be stratified equidistantly on each coordinate axis. So the resulting rank-1 lattice is an instance of a Latin hypercube sample and the minimum distance can be bounded to mindist $\geq \frac{1}{n}$.

However, the condition $\gcd(n, g_i) = 1$ prevents to find the best lattice with regard to maximized minimum distance in some cases. This also applies to searching maximized minimum distance lattices in Korobov form. For example the maximized minimum distance of the lattices of equation 3 cannot be achieved in Korobov form.

Figure 4 compares the maximized minimum distance lattices for $n = 56$ selected in Korobov form (a), for $\gcd(n, a) = 1$ in Korobov form (b) and by using the lattice family of [CR97] (c).

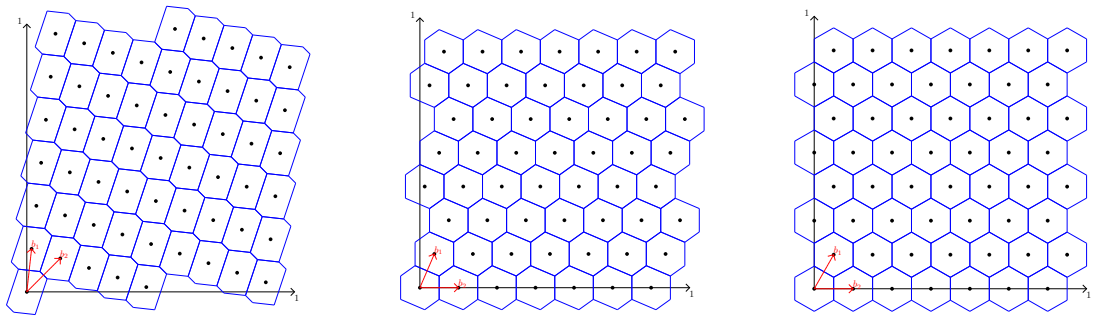

(a) $L_{56,9}$ mindist $= \frac{\sqrt{40}}{56}$

(b) $L_{56,21}$ mindist $= \frac{\sqrt{58}}{56}$

(c) $L_{56,(4,7)}$ mindist $= \frac{\sqrt{64}}{56}$

Figure 4: Maximized minimum distance lattices for $n = 56$: (a) Rank-1 lattice searched under the restriction of $\gcd(n, a) = 1$ in Korobov form. (b) Rank-1 lattice in Korobov form. (c) Rank-1 lattice selected without restrictions.

3 Quasi-Monte Carlo Error Bounds

The functions in computer graphics are square integrable due to finite energy and bounded. However, they are only piecewise continuous, where the discontinuities are difficult to identify. Often the structure of the high-dimensional integrals in image synthesis comprises several

$2-3$ dimensional integral operators, as it is the case for sampling the pixel area, the lens area, motion blur, depth of field, scattering events, etc. Consequently the sampling points can be padded using low-dimensional stratified patterns in a very efficient way, as Kollig and Keller have shown in [KK02].

The classical quasi-Monte Carlo error bound is given by the Koksma-Hlawka inequality [Nie92b], which bounds the integration error by the product of the discrepancy of the sampling points and the variation of the integrand in the sense of Hardy and Krause. However, the variation in the sense of Hardy and Krause already becomes infinite in the case of non-axis aligned discontinuities, thus being inapplicable to functions in computer graphics.

The error of a lattice rule [SJ94] can be formulated in terms of the Fourier coefficients of the integrand f requiring f to be periodic and to belong to the function class whose Fourier coefficients decay sufficiently fast with increasing frequency. Since these conditions usually do not hold for the setting of computer graphics, we cannot use this error bound either.

The notion of $(\mathcal{M}, \mu)$-uniformity introduced by Niederreiter [Nie03] supports partitions which are not axis aligned and relies on the stratification properties of the sampling points. The deterministic error bound based on this concept can easily be generalized to integro-approximation [Kel06]. Using the probability space $([0,1)^s, \mathcal{B}, \lambda_s)$, where $\mathcal{B}$ corresponds to the Borel-sets and λ_s to the s-dimensional Lebesgue-measure, this bound also applies in the context of computer graphics. However, the error cannot be separated into a property of the integrand and the sampling pattern any longer.

3.1 Error Bound for Lipschitz Functions

Although the classical error bounds do not fit in the setting of computer graphics (as seen above), quasi-Monte Carlo methods achieve good results in a vast number of numerical experiments. The main reason is that the integrands are often piecewise continuous, while the discontinuities cannot be captured by the classical error bounds. Thus they cannot explain the observed convergence. We now examine an error bound for Lipschitz continuous, periodic functions with respect to parametric integration thereby completing Niederreiter's work [Nie03] for the special case of rank-1 lattices.

Given a Minkowski-reduced basis of a rank-1 lattice $L_{n,\mathbf{g}}$ the basis vectors induce the Delaunay tessellation of the lattice and its dual, the Voronoi diagram. In order to derive the error bound we need the following

Definition 1 *The radius $r(n, \mathbf{g})$ of a rank-1 lattice is the smallest circumcircle of the fundamental Voronoi cell with respect to some suitable norm.*

This quantity corresponds to the dispersion [Nie92b]

$$d_n(L_{n,\mathbf{g}}; I^s) = \sup_{x \in I^s} \min_{1 \le i \le n} d(\mathbf{x}, \mathbf{x}_i)$$

of a rank-1 lattice as well as the notion of the covering radius in coding theory. Figure 5 shows the Voronoi diagram along with the circumcircle of radius $r(32, (1, 7))$ of the Korobov lattice $L_{32,7}$.

Based on the results of [DFG99] and by taking advantage of the geometrical properties of rank-1 lattices the proof is very simple and resembles the proofs of the paper [Nie03].

Theorem 1 *Let f be a Lipschitz function periodic on $[0,1]^{s+s'}$, with*

$$\|f(\mathbf{x}_1, \mathbf{y}) - f(\mathbf{x}_2, \mathbf{y})\| \le L\|\mathbf{x}_1 - \mathbf{x}_2\|,$$

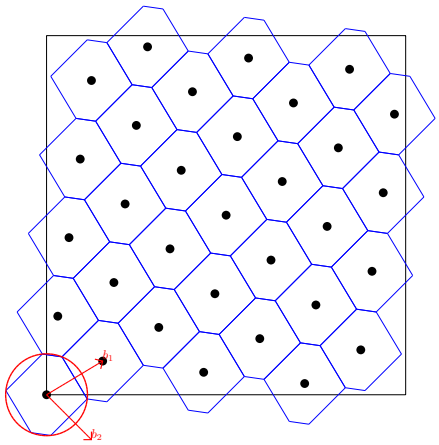

Figure 5: Voronoi diagram of the lattice $L_{32,7}$ including the basis vectors in the sense of a Minkowski-reduced basis. The circumcircle of radius $r(n, \mathbf{g})$ encloses the fundamental Voronoi cell.

and Lipschitz constant L independent of $\mathbf{x}_1, \mathbf{x}_2$ and $\mathbf{y}$, where $\dim \mathbf{x}_1 = \dim \mathbf{x}_2 = s$ and $\dim \mathbf{y} = s'$. Further let $P_n = \{\mathbf{x}_0, \ldots, \mathbf{x}_{n-1}\}$ be a rank-1 lattice. Then

$$\left\| \int_{[0,1]^s} f(\mathbf{x}, \mathbf{y}) d\mathbf{x} - \frac{1}{n} \sum_{i=0}^{n-1} f(\mathbf{x}_i, \mathbf{y}) \right\| \leq L \cdot r(n, \mathbf{g})$$

for some suitable norm, where $r(n, \mathbf{g})$ is the radius of P_n.

Proof 1 *Let $\mathcal{M} = \{M_0, \cdots, M_{n-1}\}$ be the partition of I^s by the Voronoi dia-gram of a rank-1 lattice. Then in a first step the quadrature error can be estimated similar to [DFG99]:*

$$\begin{aligned}
\left\| \int_{[0,1]^s} f(\mathbf{x}, \mathbf{y}) d\mathbf{x} - \frac{1}{n} \sum_{i=0}^{n-1} f(\mathbf{x}_i, \mathbf{y}) \right\| &= \left\| \sum_{i=0}^{n-1} \int_{M_i} (f(\mathbf{x}, \mathbf{y}) - f(\mathbf{x}_i, \mathbf{y})) d\mathbf{x} \right\| \\
&\leq \sum_{i=0}^{n-1} \int_{M_i} ||f(\mathbf{x}, \mathbf{y}) - f(\mathbf{x}_i, \mathbf{y})|| d\mathbf{x} \\
&\leq L \sum_{i=0}^{n-1} \int_{M_i} ||\mathbf{x} - \mathbf{x}_i|| d\mathbf{x} \qquad (4) \\
&= L \cdot n \int_{M_0} ||\mathbf{x}|| d\mathbf{x} \qquad (5) \\
&\leq L \cdot n \cdot \lambda_s(M_0) \sup_{\|\mathbf{x}\| \leq r(n,\mathbf{g})} ||\mathbf{x}|| \\
&= L \cdot n \cdot \frac{1}{n} \cdot r(n, \mathbf{g}) = L \cdot r(n, \mathbf{g}). \qquad (6)
\end{aligned}$$

Since the M_i are of identical shape and volume and due to the point symmetry of the lattice, we can choose $\mathbf{x}_i$ as $\mathbf{x}_0 = \mathbf{0}$ in equation (4) which then can further be simplified resulting in equation (6). □

Obviously the error bound results as a product of a property of the integrand and a property of the sampling pattern again. Omitting the parameter $\mathbf{y}$ in Theorem 1 yields the integration error bound.

Let $\Omega \subset \mathbb{R}^s$, $\mathcal{M} = \{M_0, \cdots, M_{n-1}\}$ an arbitrary tessellation of Ω, and $\{A_i\}_{i=0}^{n-1}$ the volumes of $\{M_i\}_{i=0}^{n-1}$. Then equation (4) represents the special case of the error estimation of [DFG99]

$$\left| \int_\Omega f(\mathbf{x}) d\mathbf{x} - A_i \sum_{i=0}^{n-1} f(\mathbf{x}_i) \right| \quad \leq \quad L \sum_{i=0}^{n-1} \int_{M_i} ||\mathbf{x} - \mathbf{x}_i|| d\mathbf{x} \tag{7}$$

for rank-1 lattices, where $A_i = \frac{1}{n}$. It can be proved that this error bound is minimized by choosing $\{\mathbf{x}_i\}_{i=0}^{n-1}$ and $\{M_i\}_{i=0}^{n-1}$ such that the $\{M_i\}_{i=0}^{n-1}$ are the Voronoi sets for the $\mathbf{x}_i$ and the $\mathbf{x}_i$ are the mass centroids of the Voronoi sets at the same time [DFG99]. This means that rank-1 lattices are a suitable choice to minimize the integration error for Lipschitz continuous functions, since these conditions apply to these point sets due to their geometrical properties.

The theoretical rate of the new bound $\mathcal{O}(n^{-1/s})$ is already known from the field of information based complexity and approximation theory. It obviously is cursed by the dimension, which is hidden in the radius $r(n, \mathbf{g})$. However, the important issue about this theorem is not the rate as we consider $s = 2$, but that it yields a criterion for lattice search using the primal instead of the dual lattice by means of the following corollary:

Corollary 1 *Maximizing the minimum distance*

$$d_{min}(P_n) := \min_{0 \leq i < n} \|\mathbf{x}_i\|$$

in a rank-1 lattice decreases the radius $r(n, \mathbf{g})$ and thus the integration error.

This corollary can be derived by the following observation. The minimum distance $d_{min}(P_n)$ in a rank-1 lattice corresponds to two times the radius of the in-circle of the fundamental Voronoi cell. Maximizing the minimum distance in a rank-1 lattice thus increases this radius. The Voronoi cells, being of equal size and constant volume, approximate a sphere the more, the bigger the minimum distance becomes. Consequently the gap between the radius of the circumcircle and the in-circle of the Voronoi cells decreases. This means that $r(n, \mathbf{g})$ decreases as $d_{min}(P_n)$ increases, which is stated in the corollary. Although there are similarities to sphere packings, it is important to note that this argument is not built upon them.

4 Applications

Based on the theoretical considerations of the previous sections we now investigate the effect of maximized minimum distance rank-1 lattices for integro-approximation for image synthesis and explore their geometrical properties in the context of display technology.

4.1 Anti-Aliasing by Rank-1 Lattices

A disadvantage of all current display technology that relies on regular structures to present images is that correlations between the function to be displayed and the pixel structure can

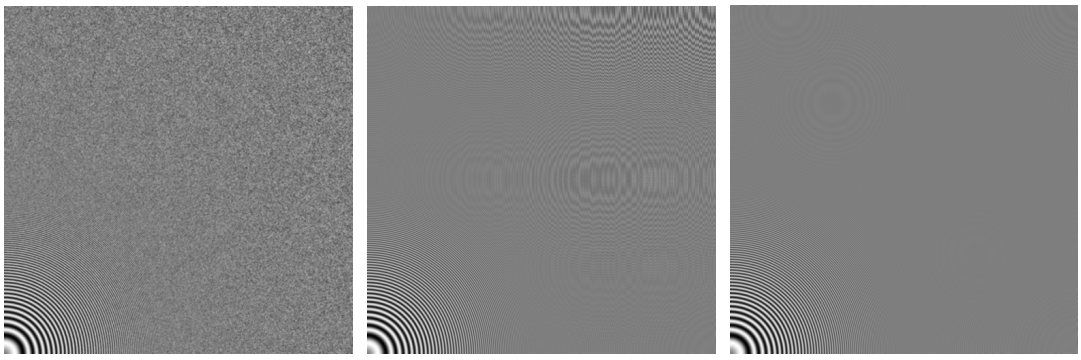

(a) Jittered grid (b) LP points (c) $L_{1048576,195638}$

Figure 6: Rendering the test function by integro-approximation with $512 \times 512 \times 4$ samples, which means that there are about 4 samples per pixel. This figure should be viewed on screen, since otherwise the differences between the images can hardly be observed due to resampling and printing.

be perceived as distorting artifacts. In order to avoid these so-called aliases, various sampling patterns have been investigated. It is common belief that at moderate sampling rates n random sampling points $\mathbf{x}_i$ with maximized minimum distance perform best, since aliases are mapped to noise, but low frequency details are reproduced clearly. Nevertheless, increasing the number of sample points can cause aliases to reappear as the noise vanishes. In fact these artifacts cannot be completely avoided because of the correlation of a deterministic display and a deterministic function, but they can be ameliorated by filtering parts of the image. However, using only a box filter, i.e. integrating over the pixel area by averaging samples, always causes aliasing to appear in an even converged image. This is illustrated in Figure 8 for the simple example of rendering an infinite checker board. As we are looking for the most efficient sampling patterns and as random sampling cannot always prevent aliasing, we investigate rank-1 lattices for image synthesis.

4.1.1 What Maximized Minimum Distance Lattices Can Do

A typical test function for anti-aliasing is given by

$$\begin{aligned} Z_2 : [0,1)^2 &\rightarrow [0,1] \\ (x,y) &\mapsto \frac{1}{2}\left(1+\sin\left(1600\cdot\left(x^2+y^2\right)\right)\right). \end{aligned}$$

Figure 6 shows the results of rendering this function by stratified sampling, the Larcher-Pillichshammer points (LP) [LP01, KK02], and the maximized minimum distance lattice $L_{1048576,195638}$ in combination with a b-spline filter of degree 3. Whereas in Figure 6 (a) the aliasing is covered by noise, Moiré patterns become clearly visible in 6 (b). The best result is achieved by the maximized minimum distance lattice, which acts as a filter due to its nice Fourier properties [SJ94]. So aliasing artifacts are attenuated considerably. In fact the maximized minimum distance lattice $L_{1048576,195638}$ with approximately 4 samples per pixel achieves a similar quality to [SSA05], where 900 samples per pixel with a density proportional to a cubic b-spline filter we used to render almost the same test function.

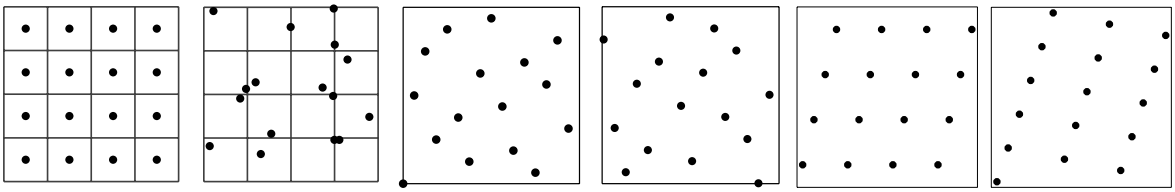

(a) Regular grid (b) Jittered grid (c) LP (d) LP rand (e) Shifted $L_{16,4}$ (f) Shifted $L_{16,3}$

Figure 7: As sampling pattern the regular and jittered grid, the Larcher-Pillichshammer (LP) and randomized Larcher-Pillichshammer points, and rank-1 lattices are used. We analyze both the maximized minimum distance rank-1 lattices in Korobov form and the lattices resulting from the condition $\gcd(n, a) = 1$. Additionally, the lattices are shifted such that the bounding box of the lattice points is centered within the pixel.

4.1.2 Speed of Convergence

In the following we compare the test patterns of Figure 7 with respect to their convergence. The sampling patterns are applied both for the integration problem (i.e. per pixel) and for the integro-approximation setting (i.e. over the whole quadratic screen). The test scene is given by the checker board of Figure 8(a).

In order to analyze the convergence of the test patterns, the L_2-norm of a converged reference image to the corresponding test image is computed for an increasing number of sampling points per pixel. Then the resulting value is diagrammed in the error graph, displaying the number of samples on the x- and the error norm on the y-axes. Both axis are scaled logarithmically. The reference image, shown in Figure 8(b), was computed by applying a jittered grid sampling pattern with 1024×1024 samples at each pixel. Obviously there are still aliasing artifacts in this image resulting from the problem of rendering a deterministic function on a deterministic display.

It is important to note that there are two different visual artifacts in image 8(a). The first one results from the case of only one edge lying in a single pixel. At low sampling rates these edges appear very jagged. Increasing the sampling rate solves this problem, though. Walking towards the horizon of the checker board, the single cells of the checker board get smaller and smaller. Therefore, many small cells, i.e. many edges fall within one pixel near the horizon as shown in Figures 8 (e) and (f), yielding the aliasing structures in the converged image. Thus, we compute the error graphs only for the lower half of the checker board scene, where the convergence to the correct image is guaranteed.

Integration We start by applying the test patterns (Figure 7) per pixel. For each pixel n rays are shot from the camera into the screen and the resulting color values are averaged by means of the box filter. Although the regular grid possesses a worse discrepancy than the Larcher-Pillichshammer or lattice points, we notice that it performs extremely well, even surpassing them for certain n. This can be explained by the discrepancy being an anisotropic measure in fact. The large error spikes in Figure 9 arise from the factorization of n, since it is not always possible to find a good one. Jittered grid sampling turns aliasing into noise, and thus, the error proceeds on a lower level. However, this sampling pattern suffers from the same factorization problem as the regular grid.

The idea of using rank-1 lattices for computing the pixel integral is already mentioned

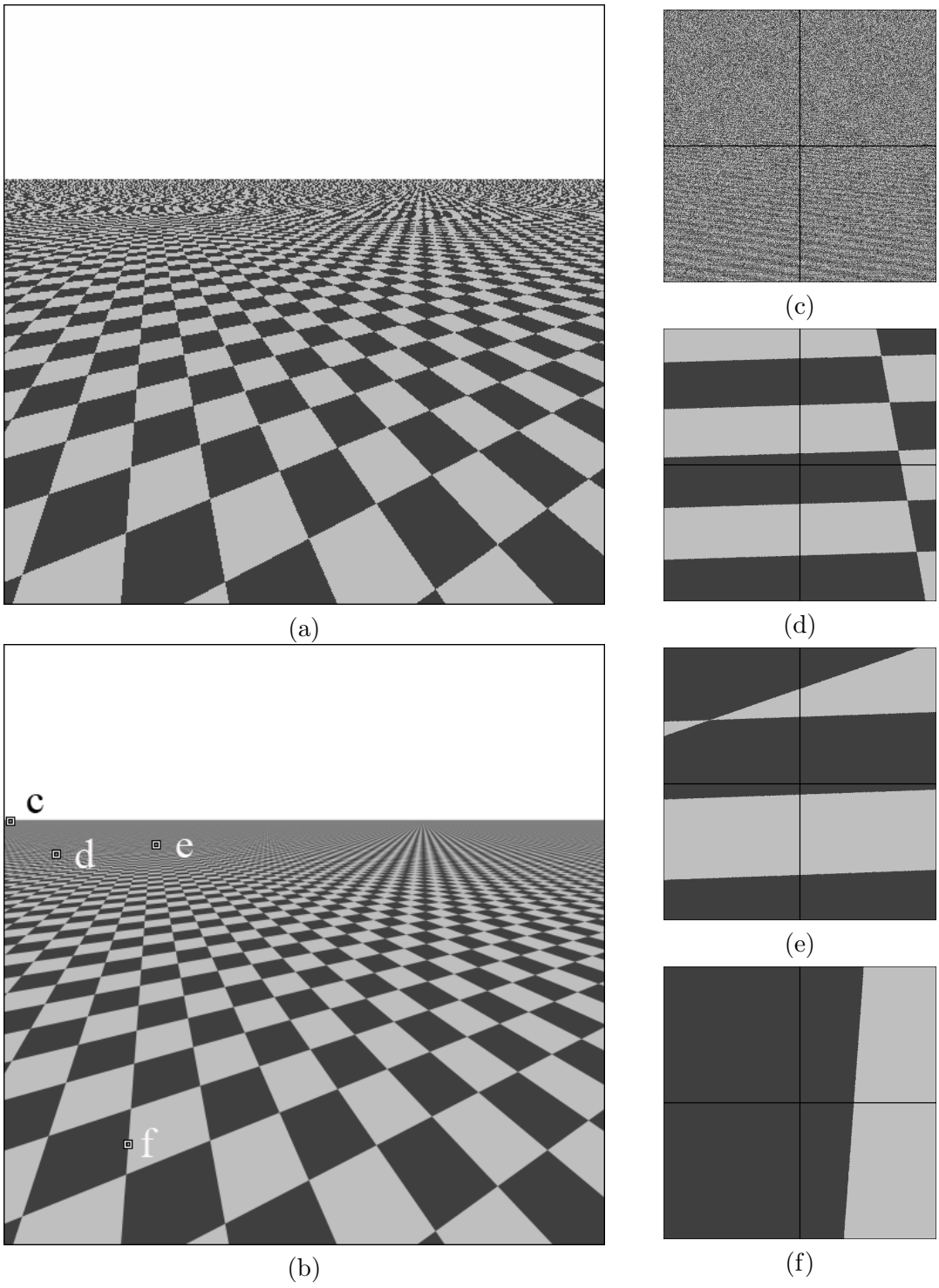

Figure 8: (a) Aliasing due to the discrete representation of the checker board.
(b) Reference image used to determine the L_2 error. (c)-(f) Magnification of the highlighted areas of (b), comprising 2×2 pixels each: (c) Roughly the same number of light and dark gray checker board cells cover this area averaging to half gray in (b). (d) The light and dark gray cells do not cover the same area in the pixels leading to aliasing. (e) The light and dark gray cells do not cover the same area in the pixels leading to aliasing. (f) Two pixels are completely covered by one dark gray cell, whereas an edge between two cells runs through the other two.

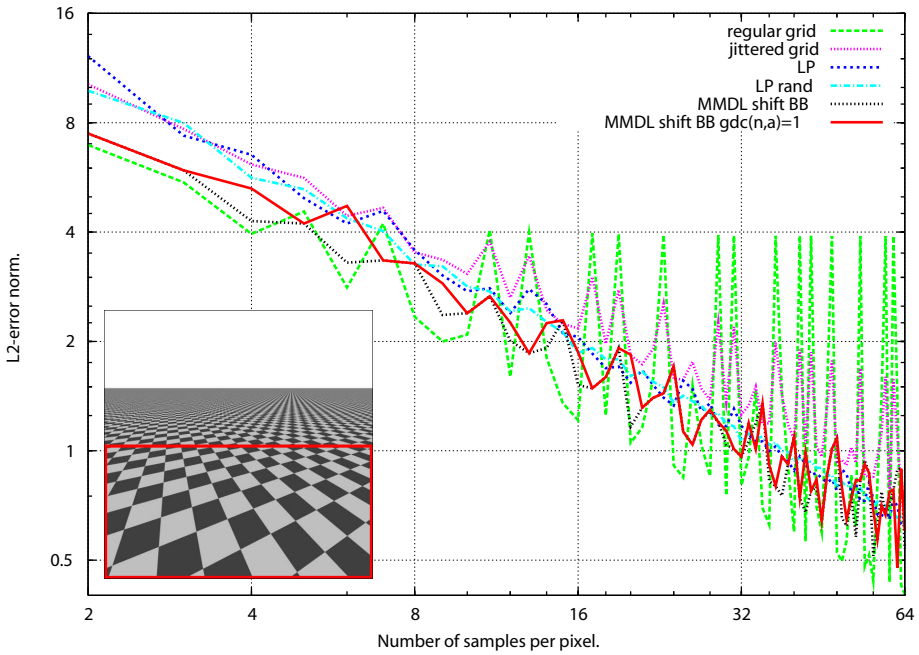

Figure 9: Comparison of the regular and jittered grid, the Larcher-Pillichshammer points, shifted maximized minimum distance lattices and the maximized minimum distance lattices with $\gcd(n, a) = 1$.

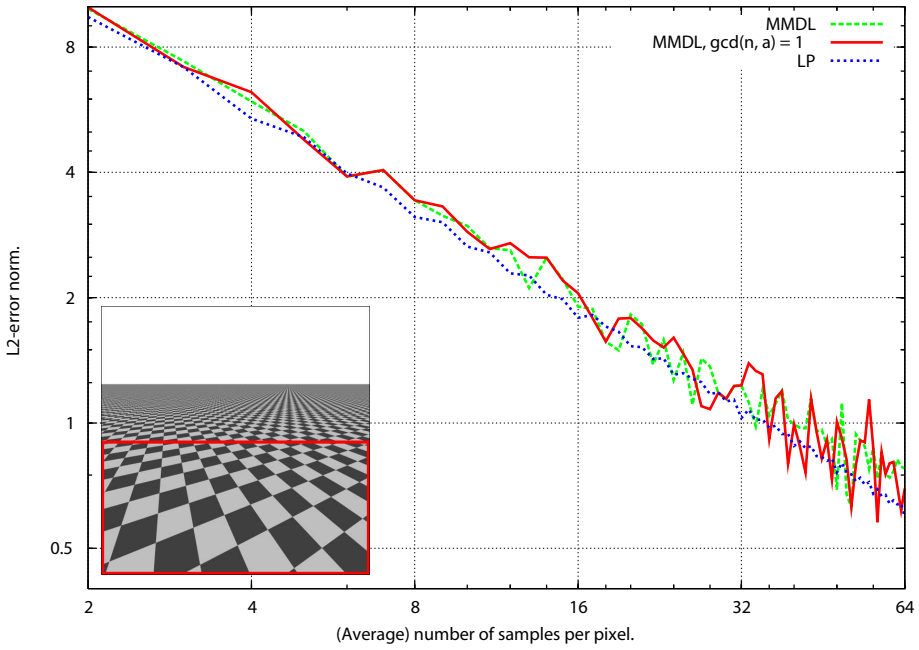

Figure 10: Comparing the Larcher-Pillichshammer points and maximum minimum distance lattices scaled to the whole screen.

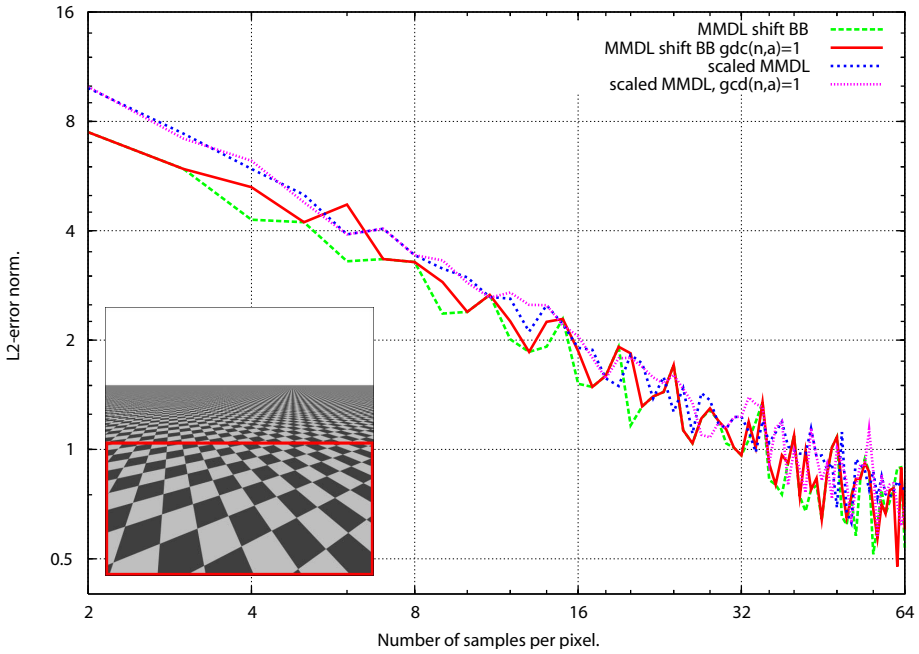

Figure 11: Comparison integration/integro-approximation for the rank-1 lattices.

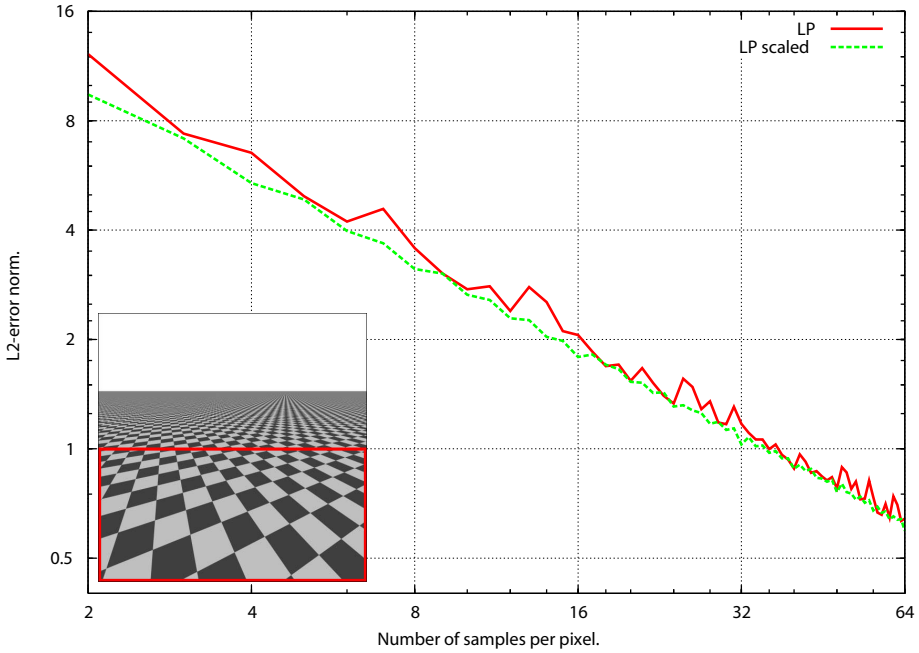

Figure 12: Comparison integration/integro-approximation for the Larcher-Pillichshammer points.

in [Nie92a], however, not with respect to maximized minimum distance. Examining the maximized minimum distance lattices, we observe that postulating $\gcd(n, a) = 1$ sometimes severely restricts the search space; e.g. for $n = 4$ we get the pixel diagonal as sampling pattern which clearly is not a good distribution. Altogether the error curves expose a relatively strong oscillation. This is due to the structure of the lattice points featuring families of hyperplanes which are sometimes aligned to the checker board edges in such a way that these cannot be captured. As the Larcher-Pillichshammer points do not suffer from this, clearly scene dependent, problem, they offer a relatively smooth error curve.

Integro-Approximation Next we use the Larcher-Pillichshammer points and maximized minimum distance lattices over the whole quadratic screen ($xRes = yRes$), i.e. these sampling patterns are scaled from $[0, 1)^2$ to $[0, xRes) \times [0, yRes)$. To obtain a certain number n of samples per pixel, the number of sampling points has to be chosen as $xRes \cdot yRes \cdot n$. Since the Larcher-Pillichshammer pattern for $n = 2^m$ points represents a $(0, m, 2)$-net in base $b = 2$, we can guarantee a certain number of samples per pixel if the screen resolution is chosen as a power of 2. If the number of sampling points equals $xRes \cdot yRes \cdot k = 2^m$ for $k = 1$, we can take each pixel as an elementary interval of volume $b^{-m} = 2^{-m} = \frac{1}{xRes} \cdot \frac{1}{yRes}$. For $k > 1$, each pixel contains k elementary intervals of volume $\frac{1}{xRes} \cdot \frac{1}{yRes} \cdot \frac{1}{k}$. So each pixel is sampled by the same number of points, with each pixel being sampled by a different pattern at the same time. Considering the correlation between the pixels, the scaled Larcher-Pillichshammer points obtain an even smoother error curve than in the integration setting, as can be seen in Figure 12. This is even true for the case $n \neq 2^m$.

In contrast to the Larcher-Pillichshammer points, the rank-1 lattices cannot achieve the same number of sampling points per pixel and the image becomes quite noisy, especially for low sampling rates. Moreover, there are again orientations in the checker board, which fall exactly between two hyperplanes, resulting in an oscillating integration error. This also affects the comparison to the integration setting. So, in contrast to the Larcher-Pillichshammer points, the error graph for the integro-approximation problem is slightly worse than the one of the integration setting, which is illustrated in Figure 11.

Altogether, the test patterns converge to the reference image, which still exposes aliasing in the case of using the box filter for integration. The Larcher-Pillichshammer and maximized minimum distance sampling patterns show the fastest convergence rate, with the first outperforming the latter for this test scene.

4.2 Images on Rank-1 Lattices

A raster display is typically formed from a matrix of pixels representing the whole screen. Whereas a pixel is usually represented as a square on the integral raster being defined by the display resolution, we now structure the pixel layout by the Voronoi diagram of a maximized minimum distance rank-1 lattice, i.e. the single picture elements are represented as the cells which are induced by the Voronoi diagram of the rank-1 lattice points.

This kind of display technology has several advantages. Since rank-1 lattices are available for any number n of points, the number of pixels can be chosen freely. As seen in Section 2.2 maximizing minimum distance approximates a hexagonal grid in the limit yielding almost hexagonal picture elements. The concept of hexagonal pixels has already been studied in the context of hexagonal image processing ([MS05]) and is used in the SmartSlab LED panels (www.metropolismag.com). Moreover, this pixel layout permits optically better results than

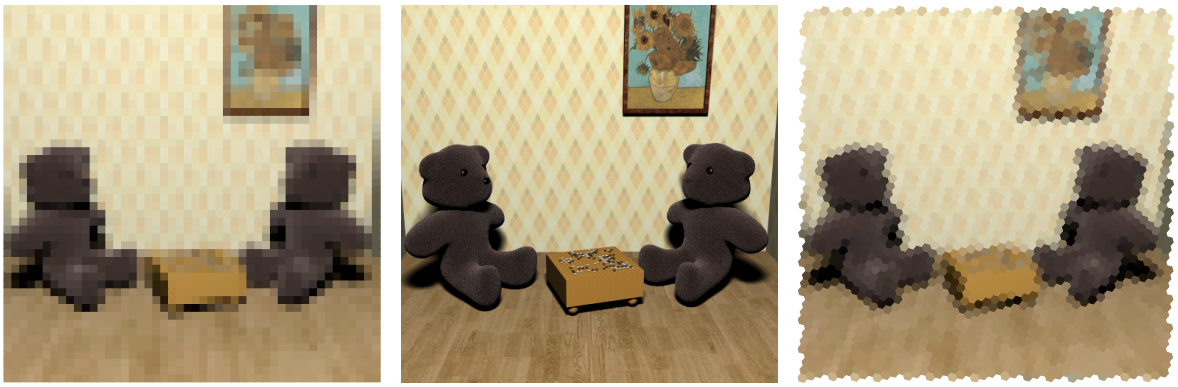

Traditional display, 48×48 pixels | Original image, 512×512 pixels | Rank-1 lattice display, 48×48 pixels

Figure 13: Comparison of rank-2 (left) and maximized minimum distance rank-1 lattice (right) displays at identical pixel resolution for approximating the high resolution image in the middle.

rank-2 lattices, as for example a smoother representation of curved objects. This can be seen in Figure 13, where the original image (middle) has been computed in reduced resolution, once on a traditional rank-2 lattice and once on a maximized minimum distance rank-1 lattice. At the same time, image processing algorithms are simplified in comparison to hexagonal lattices. In the same way image processing algorithms which are based upon the fast Fourier transform become simpler and can be implemented in a slightly more efficient way [DKD07].

This concept can technically be realized in a number of ways: One possibility consists in making up the display of point light sources, like for example RGB LEDs, which are arranged in the center of each Voronoi cell. Composing the display of area light sources which cover the single picture elements yields a technique for TFT and LCD displays, respectively. This may be realized by means of OLEDs for instance. Moreover, the layout of the sensors, i.e. the photosites, of a CCD (Charge-Coupled Device) camera can take the form of a rank-1 lattice cell. Further applications are given by projector technology, $3d$-Displays, etc.

4.2.1 2^n Display Modules, Sensors, and Images

Since rank-1 lattices can be tiled seamlessly, it is possible to compose a display of k modules each of which having the same number of lattice cells. This is illustrated in Figure 14.

The idea of 2^n display modules consists in choosing the number of picture elements for one display module as a power of 2. This has the advantage that the single cells easily can be addressed by means of a demultiplexer. If the number k of modules is set to a power of 2 as well, the single modules can be controlled the same way.

Such displays can be produced quite cheaply by fabricating small modules of the same layout and the same number of lattice cells which can easily be assembled to a display of desired resolution. More generally, the concept of 2^n displays perfectly fits all aspects of computer technology, taking advantage of memory layout, cache lines, addressing, etc.

Storing images according to this scheme leads to the concept of 2^n images which equally benefit from the advantages of 2^n displays. The $\mathcal{O}(2^n)$ memory requirements ideally fit paging (memory alignment). As a further example storing a sequence of textures as $2^0 \cdots 2^n$ images

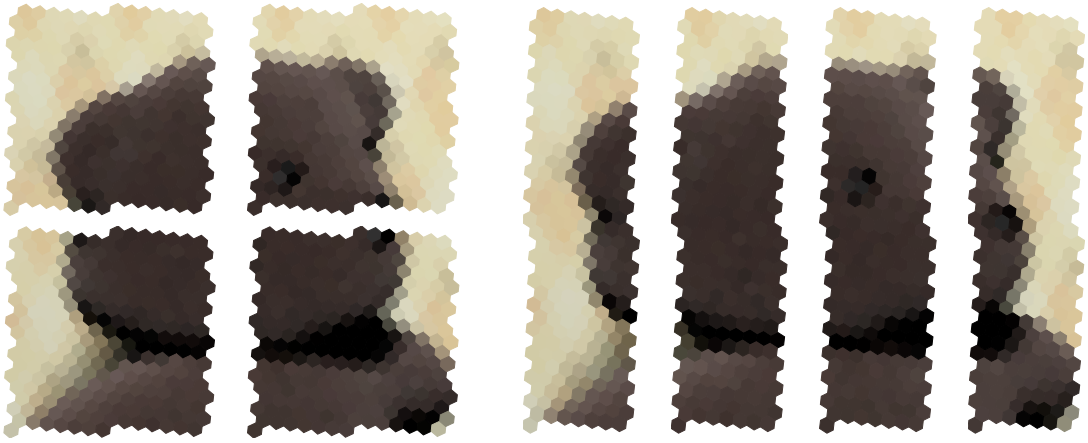

Figure 14: The display is composed of 4 modules each of which contains 256 cells. Left: Quadratic layout of the single modules, i.e. the rank-1 lattice is searched on the unit square. Right: Rectangular layout, i.e. the rank-1 lattice is searched on a rectangular domain by means of a corresponding weighted norm.

naturally supports MipMapping and allows for a simple fast Fourier transforms [DKD07] processing.

4.2.2 Rasterization

Mathematical (ideal) primitives, such as lines, triangles, or circles are usually described in terms of 2-dimensional vertices on a Cartesian grid. In order to render them correctly a so-called rasterizer approximates them by assigning the appropriate colors to sets of pixels [FvDFH96]. The rasterizer converts the two-dimensional vertices in screen space into pixels on the display.

Changing the pixel layout by the introduction of rank-1 lattice displays also yields new algorithms for rasterization. Instead of rasterizing on a rectangular grid, the rasterization is now performed on the Voronoi cells of a maximum distance rank-1 lattice.

The basic idea for converting the traditional rasterization algorithms to rank-1 lattices simply consists in changing the basis in which the rasterization is performed. This means that the rasterizer switches from the Cartesian coordinate system to that coordinate system which is formed by the basis of the corresponding rank-1 lattice. Whereas this method can be simulated on traditional raster displays by means of a software solution, it can even be performed on current graphics hardware in the following way: Since the rasterizer is only capable of operating on rectangular grids, in a first step the scene has to be transformed into the lattice basis, which in fact corresponds to a shear of the rectangular grid. After this change of frame the rasterization can be performed on the graphics hardware as usual. In order to display the rasterized scene, the resulting image has to be transformed back into the pixel basis. Performing the rasterization directly on a rank-1 lattice would have yielded the same result.

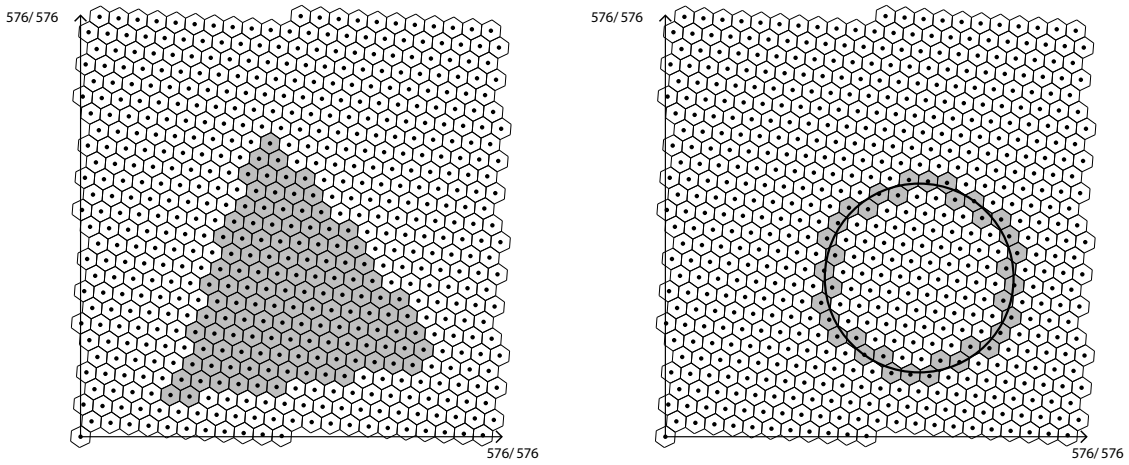

Figure 15: Examples for rasterizing a triangle and a circle on the lattice $L_{576,155}$.

5 Conclusion

We examined maximized minimum distance rank-1 lattices in the context of integro-approximation and display technology. We derived an error bound for the class of Lipschitz continuous, periodic functions. Numerical experiments proved that these lattices perform quite well in image synthesis. However, the visual results are mixed: On the one hand extreme performance and quality gains were observed, on the other hand the convergence rate heavily depends on the function class, as the checker board example showed. Due to their algorithmical simplicity, maximized minimum distance rank-1 lattices are very promising with regard to data layout and image processing at a power of 2 pixels.

6 Acknowledgments

The authors would like to thank mental images GmbH for support and for funding of this research. The authors are very thankful for the very fruitful communication with Fred Hickernell and Ronald Cools.

References

[AEVZ02] E. Agrell, T. Eriksson, A. Vardy, and K. Zeger. Closest point search in lattices. *IEEE Transactions on Information Theory*, 48(8):2201–2214, 2002.

[BN83] I. Borosh and H. Niederreiter. Optimal multipliers for pseudo-random number generation by the linear congruential method. *BIT*, 23:65–74, 1983.

[CR97] R. Cools and A. Reztsov. Different quality indexes for lattice rules. *Journal of Complexity*, 13(2):235–258, 1997.

[DFG99] Q. Du, V. Faber, and M. Gunzburger. Centroidal Voronoi tessellations: Applications and algorithms. *SIAM Rev.*, 41(4):637–676, 1999.

[DKD07] H. Dammertz, A. Keller, and S. Dammertz. Simulation on Rank-1 Lattices. In A. Keller, S. Heinrich, and H. Niederreiter, editors, *Monte Carlo and Quasi-Monte Carlo Methods 2006*. Springer, in this volume.

[FvDFH96] J. Foley, A. van Dam, S. Feiner, and J. Hughes. *Computer Graphics, Principles and Practice, 2nd Edition in C*. Addison-Wesley, 1996.

[HA90] P. Haeberli and K. Akeley. The Accumulation Buffer: Hardware Support for High-Quality Rendering. In *Computer Graphics (SIGGRAPH 90 Conference Proceedings)*, pages 309–318, 1990.

[Kel97] A. Keller. Instant Radiosity. In *SIGGRAPH 97 Conference Proceedings*, Annual Conference Series, pages 49–56, 1997.

[Kel06] A. Keller. Myths of Computer Graphics. In H. Niederreiter and D. Talay, editors, *Monte Carlo and Quasi-Monte Carlo Methods 2004*, pages 217–243. Springer, 2006.

[KH01] A. Keller and W. Heidrich. Interleaved Sampling. In K. Myszkowski and S. Gortler, editors, *Rendering Techniques 2001 (Proc. 12th Eurographics Workshop on Rendering)*, pages 269–276. Springer, 2001.

[KK02] T. Kollig and A. Keller. Efficient Multidimensional Sampling. *Computer Graphics Forum*, 21(3):557–563, September 2002.

[Knu81] D. Knuth. *The Art of Computer Programming Vol. 2: Seminumerical Algorithms*. Addison Wesley, 1981.

[LP01] G. Larcher and F. Pillichshammer. Walsh Series Analysis of the L_2-Discrepancy of Symmetrisized Point Sets. *Monatsh. Math.*, 132:1–18, 2001.

[MS05] L. Middleton and J. Sivaswamy. *Hexagonal Image Processing: A Practical Approach (Advances in Pattern Recognition)*. Springer-Verlag, 2005.

[Nie86] H. Niederreiter. Dyadic fractions with small partial quotients. *Monatsh. Math*, 101:309–315, 1986.

[Nie92a] H. Niederreiter. Quasirandom Sampling in Computer Graphics. In *Proc. 3rd Internat. Seminar on Digital Image Processing in Medicine, Remote Sensing and Visualization of Information (Riga, Latvia)*, pages 29–34, 1992.

[Nie92b] H. Niederreiter. *Random Number Generation and Quasi-Monte Carlo Methods*. SIAM, Philadelphia, 1992.

[Nie03] H. Niederreiter. Error bounds for quasi-Monte Carlo integration with uniform point sets. *J. Comput. Appl. Math.*, 150:283–292, 2003.

[SIP06] B. Segovia, J. Iehl, and B. Péroche. Non-interleaved Deferred Shading of Interleaved Sample Patterns, September 2006. Eurographics/SIGGRAPH Workshop on Graphics Hardware '06.

[SJ94] I. Sloan and S. Joe. *Lattice Methods for Multiple Integration*. Clarendon Press, Oxford, 1994.

[SSA05] M. Stark, P. Shirley, and M. Ashikhmin. Generation of stratified samples for b-spline pixel filtering. *Journal of Graphics Tools*, 10(1):39–48, 2005.

[Yel83] J. Yellot. Spectral Consequences of Photoreceptor Sampling in the Rhesus Retina. *Science*, 221:382–385, 1983.